PANDORA

Why are the photo-nuclear reaction data so mutually inconsistent?
— a survey on the photo-nuclear reaction data —

Ultra-high-energy Cosmic Rays

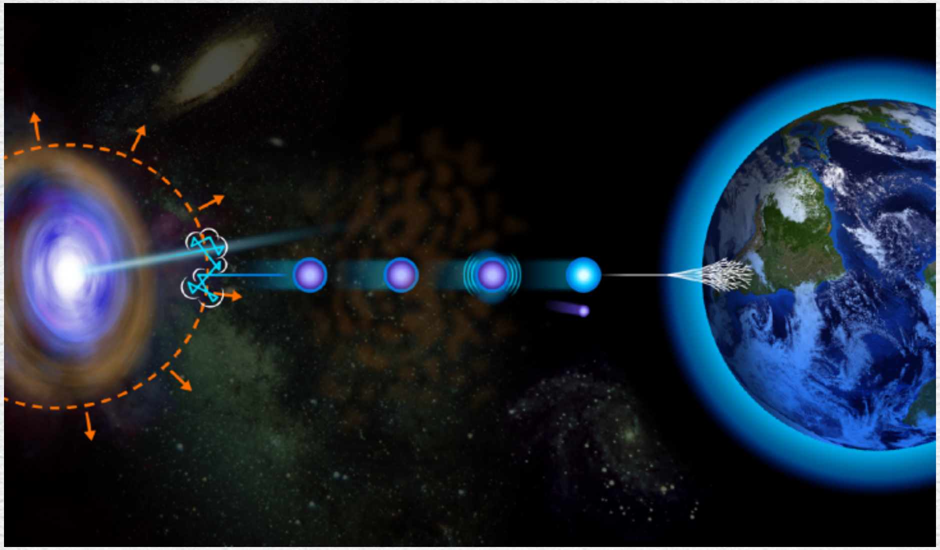

Experimental Data

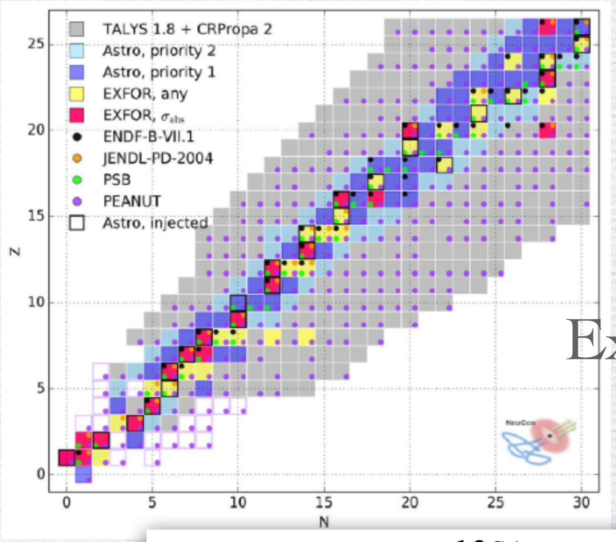

Extragalactic propagation

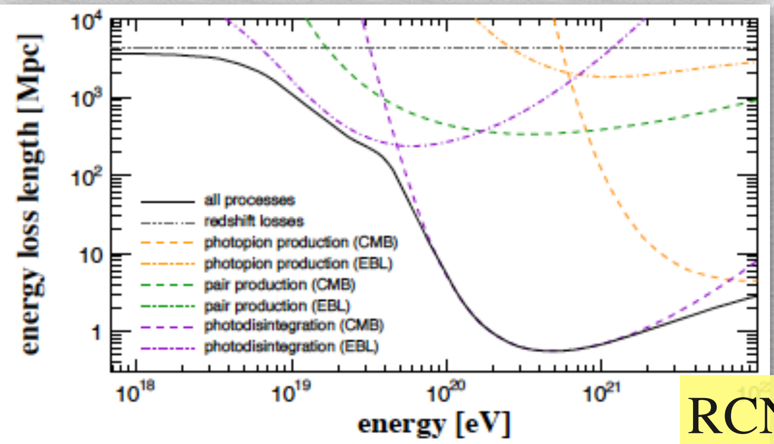

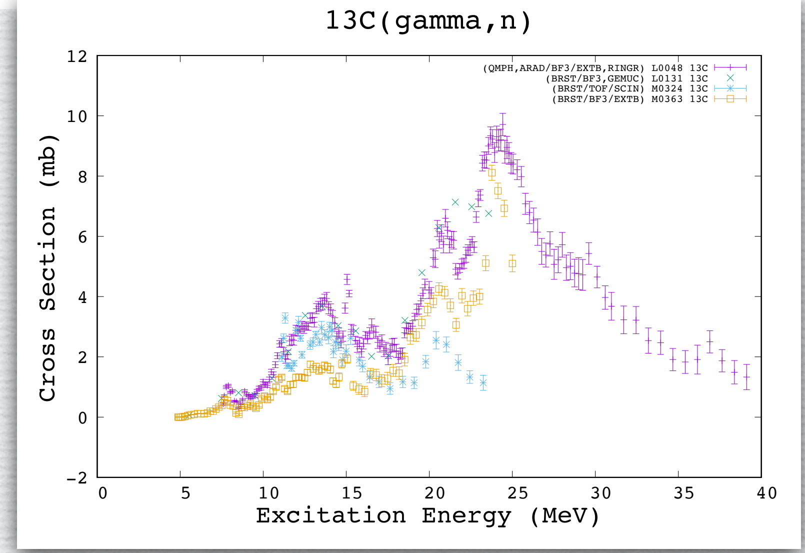

RCNP核理1aグループ勉強会 2020.5.21 by A. Tamii

Motivation

PANDORA Project

The origin and acceleration mechanism of ultra high energy cosmic rays (UHECR) (>10^{18}) eV is still not understood.

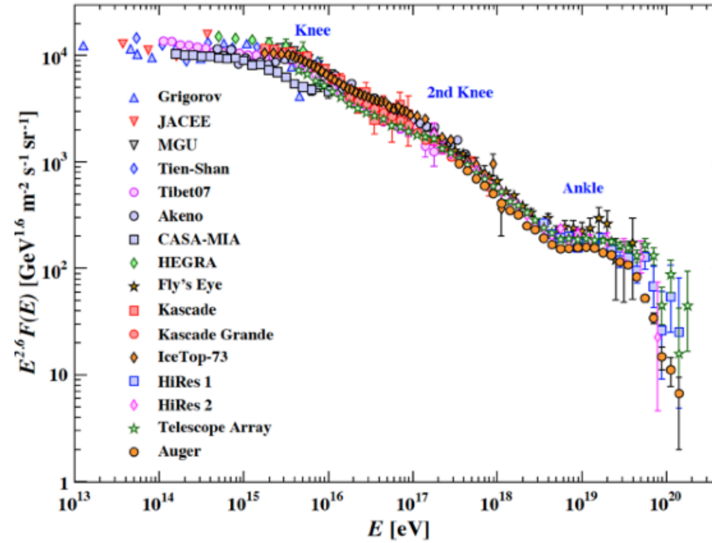

The energy UHECR nuclei is governed by photo-disintegration process by the collision with

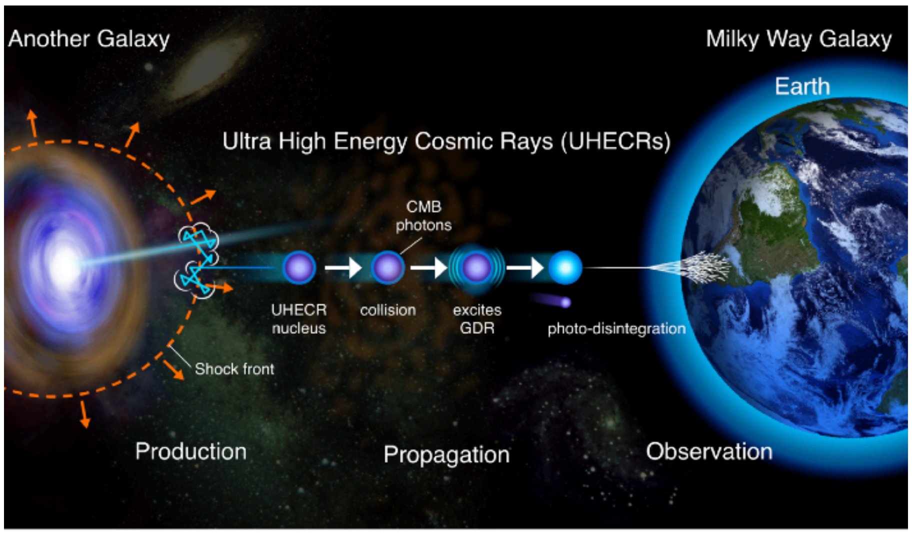

13C(gamma,n)

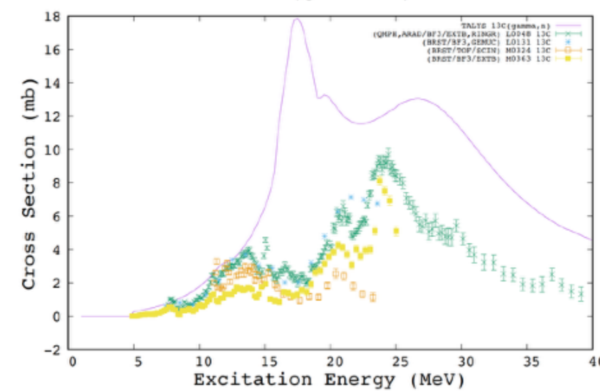

Systematic data or reliable theoretical descriptions are required for the photo-absorption cross section and decay branching ratios of stable nuclei up to A~56.

Data are scarce.

Available data are often mutually inconsistent.

Insufficient predictability by theoretical models.

Systematic measurement

Development o f nuclear theories

PANDORA Project

Photo-**A**bsorption of **N**uclei and **D**ecay **O**bservation for **R**eactions in **A**strophysics

Systematic Measurement on E1 Strength Distribution and n,p,α,γ decays up to A~56

RCNP-Grand Raiden

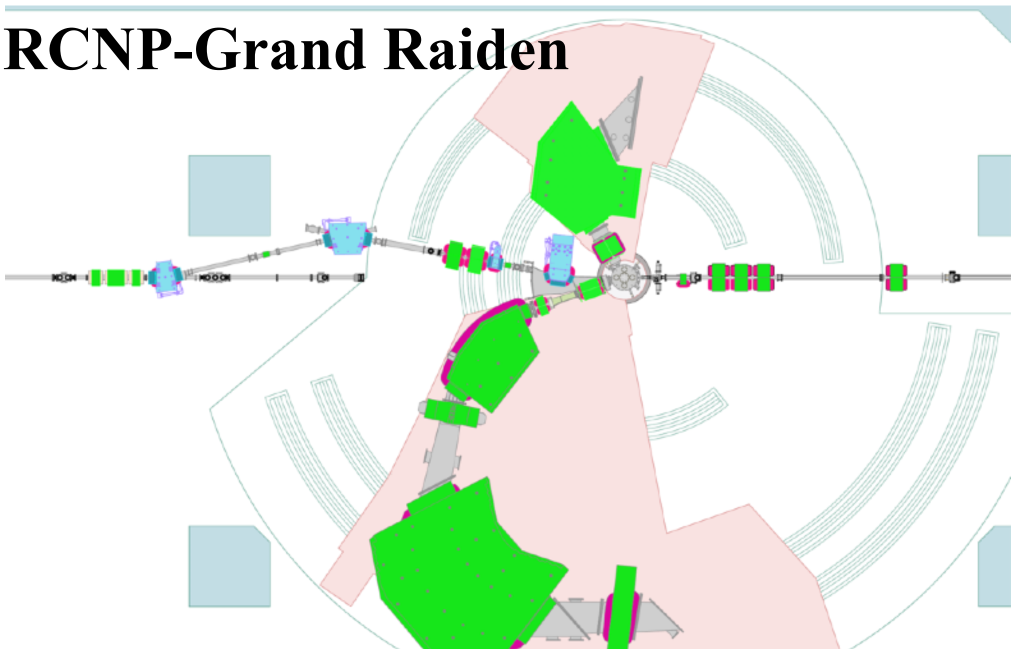

iThemba LABS

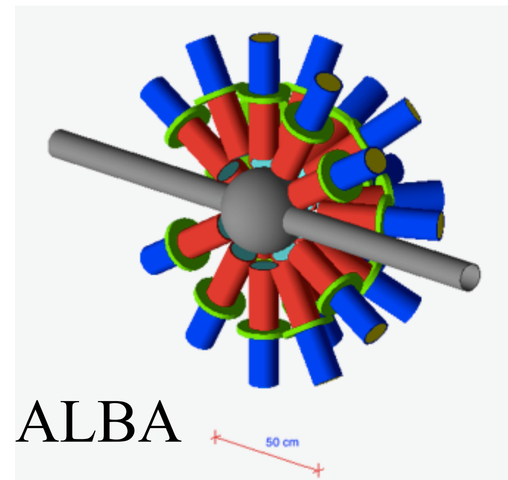

ELI-NP

Combination of experiments with complementary devices.

CAKE

decay charge particle detector array

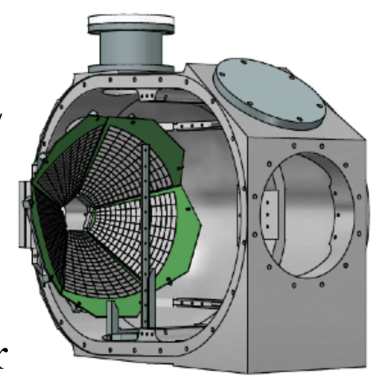

Probing Photo-Nuclear Response of Nuclei

with new technologies

Virtual photo excitation by proton scattering

- Missing mass method
  with proton Coulomb excitation

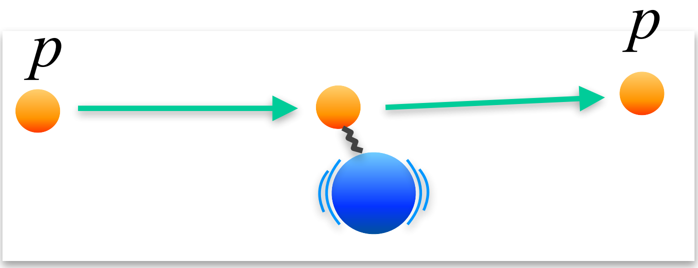

- better for total strength
  and strength distribution
  higher cross sections
  also applicable for p,α,γ decays

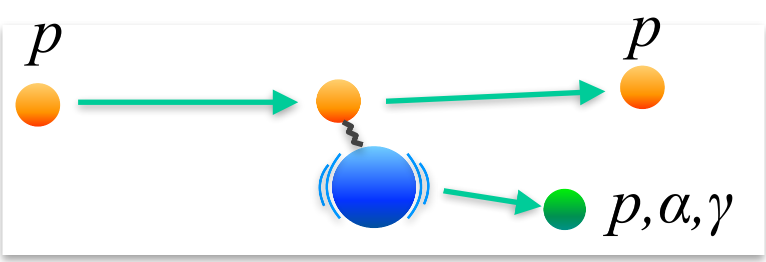

Real photo excitation

- Gamma-beam by laser-Compton
  scattering with an electron beam

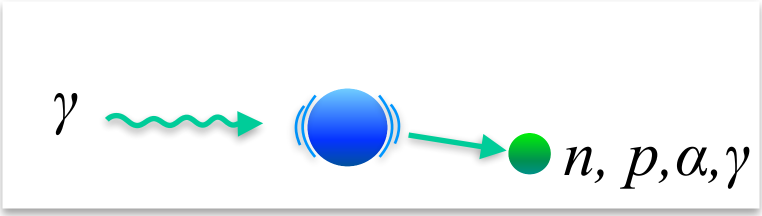

- individual decay channels
  better for absolute normalization
  applicable also for *n* and *xn* decays in addition to p,α,γ

Summary

Quasi mono-energetic gamma-rays or excitation energy tagging is required.

$\Delta E \leq$ 100-200 keV

Good absolute c.s. normalization is required.

Lack of the way of measuring total photo absorption c.s. (for isotopically enriched material) needs to be overcome.

Applicability to isotopically enriched (small amount of) target material is required.

Experimental Methods

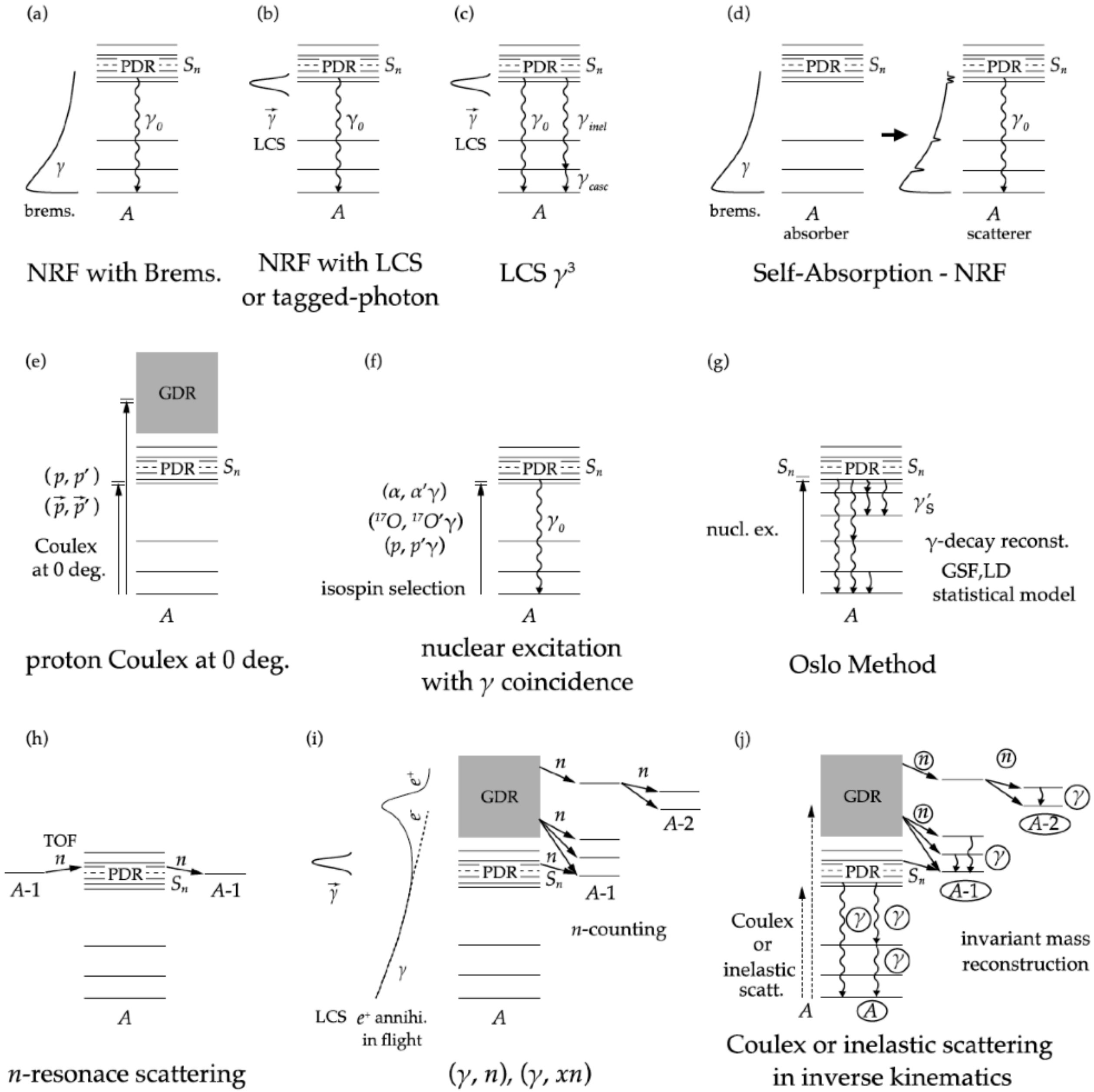

A. Bracco, E.G. Lanza and AT, PPNP 106, 360 (2019)

Sources

Bremsstrahlung

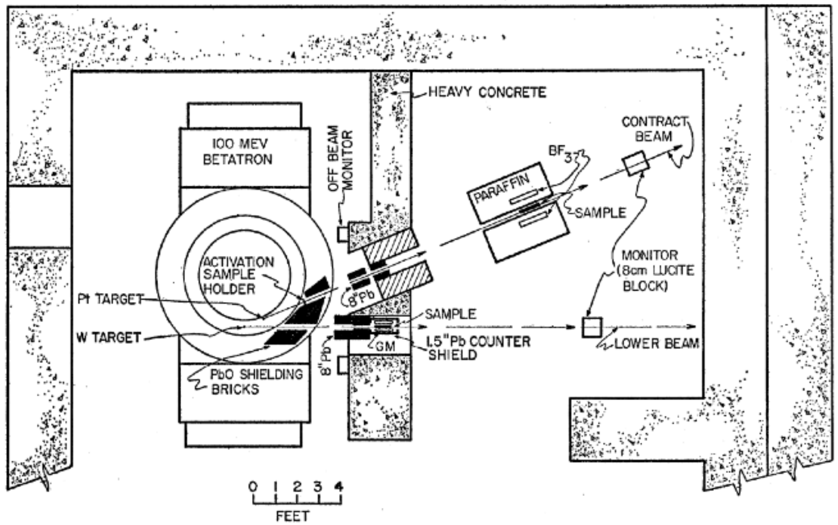

Positron annihilation in flight

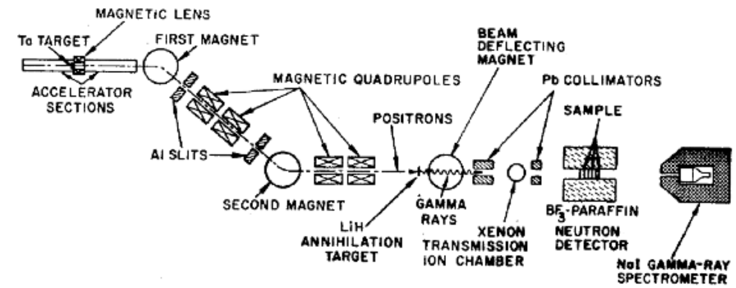

FIG. 1. Experimental apparatus for photoneutron cross-section measurements. The drawing is not to scale. Neutron shields and some gamma-ray shielding have been omitted.

Laser Compton Source (LCS)

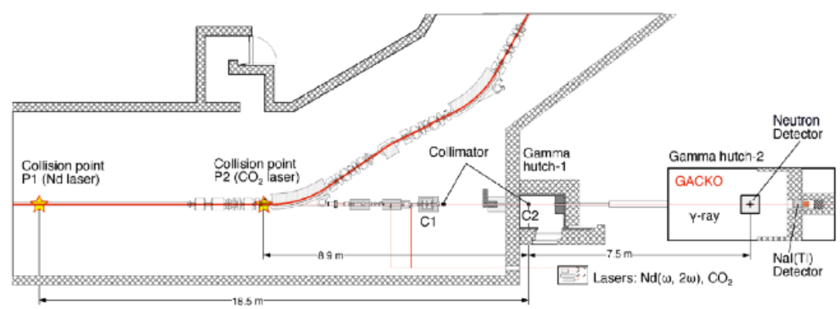

FIG. 2. (Color online) The γ-ray beam-line BL01 of the NewSUBARU synchrotron radiation facility.

Tagged-photon (bremsstrahlung tagging)

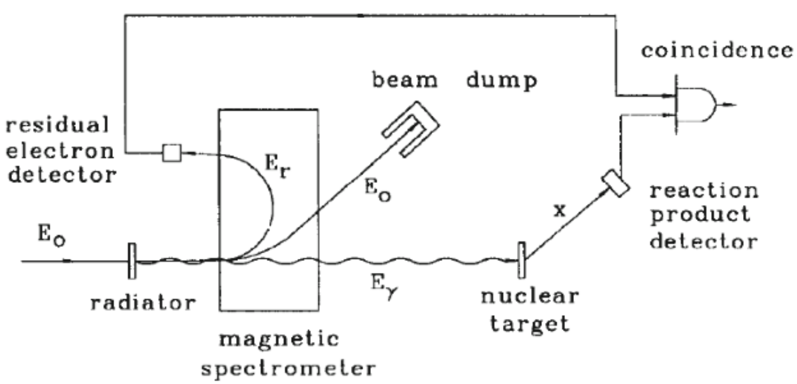

Photo-absorption C.S. is not (γ,xn) for light-medium heavy nuclei

^{208}Pb

AT et al., PRL107, 062502 (2011)

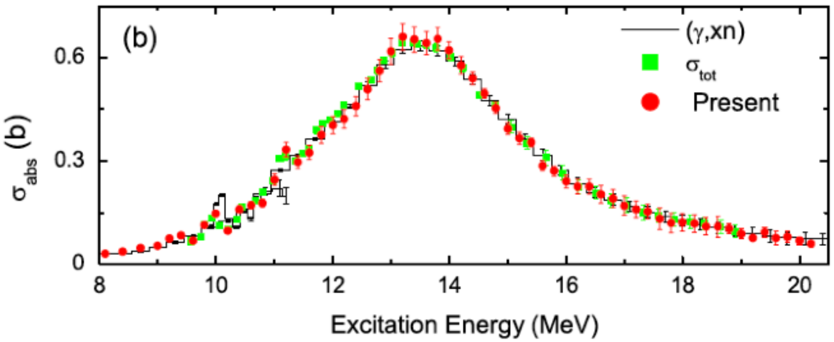

^{16}O

E.G. Fuller, Phys. Rep 127, 185 (1985)

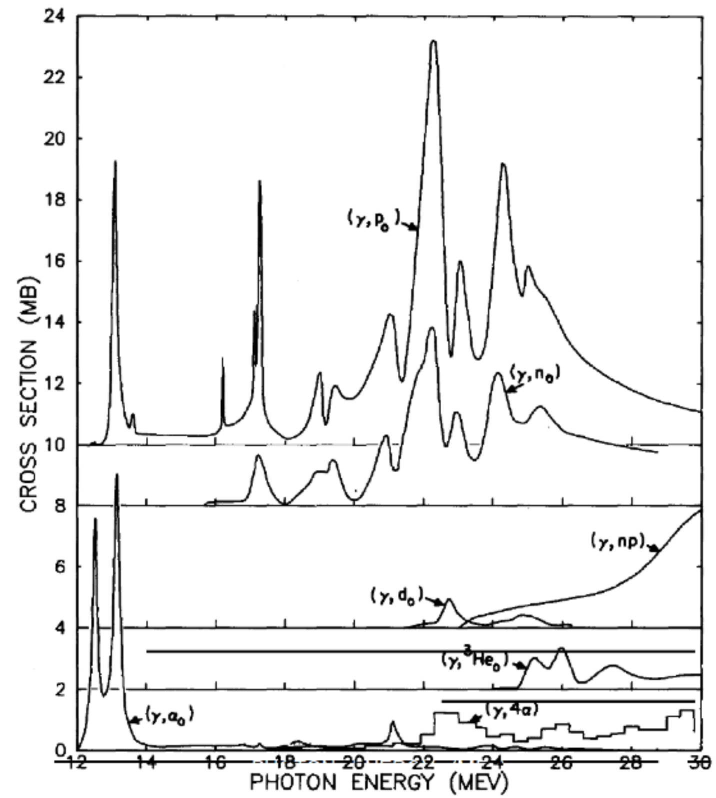

Fig. 4.6. Comparison of the ground-state photoproton and photoneutron cross sections with those for the small component reactions. Symbols associated with each of the curves indicate the reaction plotted. The quantities plotted for each reaction are: (γ, α_0), $3\times\sigma(E)$; $(\gamma, 4\alpha)$, $3\times\sigma(E)$; $(\gamma, {}^3He_0)$, $6\times\sigma(E)+2.0$; (γ, d_0), $3\times\sigma(E)+4.0$; (γ, np), $3\times\sigma(E)+4.0$; (γ, n_0), $\sigma(E)+8.0$; (γ, p_0), $\sigma(E)+10.0$.

Definitions

$$\begin{aligned}
\sigma_{1nX} &\equiv \sigma(\gamma, 1nX) \\
&= \sigma(\gamma, 1n) + \sigma(\gamma, np) + \sigma(\gamma, n\alpha) + \dots \ , \quad (1)
\end{aligned}$$

$$\begin{aligned}
\sigma_{xn} &\equiv \sigma(\gamma, xn) \\
&= \sigma(\gamma, 1n) + \sigma(\gamma, np) + \sigma(\gamma, n\alpha) + \dots \\
&+ 2\sigma(\gamma, 2n) + 2\sigma(\gamma, 2np) + 2\sigma(\gamma, 2n\alpha) + \dots \\
&+ 3\sigma(\gamma, 3n) + 3\sigma(\gamma, 3np) + 3\sigma(\gamma, 3n\alpha) + \dots, \\
&= \sum_i i\sigma_{inX} \ , \qquad (2)
\end{aligned}$$

$$\begin{aligned}
\sigma_{Sn} &\equiv \sigma(\gamma, Sn) \\
&= \sigma(\gamma, 1n) + \sigma(\gamma, np) + \sigma(\gamma, n\alpha) + \dots \\
&+ \sigma(\gamma, 2n) + \sigma(\gamma, 2np) + \sigma(\gamma, 2n\alpha) + \dots \\
&+ \sigma(\gamma, 3n) + \sigma(\gamma, 3np) + \sigma(\gamma, 3n\alpha) + \dots \\
&= \sum_i \sigma_{inX} \ . \qquad (3)
\end{aligned}$$

$$\begin{aligned}
\sigma_{abs} &\equiv \sigma(\gamma, abs) \\
&= \sigma_{Sn} + \sigma(\gamma, p) + \sigma(\gamma, 2p) + \dots + \\
&+ \sigma(\gamma, d) + \sigma(\gamma, dp) + \cdots + \sigma(\gamma, \alpha) + \dots \quad (4)
\end{aligned}$$

also fissions..

T. Kawano et al., Nucl. Data Sheets 163, 109 (2020)

EXFOR Abbreviations

detector

1 BAF2 Scintillator BaF2
2 BF3 Boron Trifluoride neutron detector
3 BGO Bismuth-Germanate crystal detector
4 BPAIR Electron-pair spectrometer
5 BUBLC Bubble chamber
6 CEREN Cerenkov detector
7 COIN Coincidence counter arrangement
8 COMPL Compton Polarimeter
9 CSICR Cesium-Iodide crystal
10 D4PI 4pi detector
11 DRFTC Drift chamber
12 FISCH Fission chamber
13 GE Germanium detector
14 GE-IN Germanium intrinsic detector
15 GELI Germanium-Lithium detector
16 GEMUC Geiger-Mueller counter
17 GLASD Glass detector
18 HE3SP He-3 spectrometer
19 HORBU Hornyak button detector
20 HPGE Hyperpure Germanium detector
21 IMPSI Passivated implanted planar Si detector
22 IOCH Ionization chamber
23 LEGE Low energy Germanium Detector
24 LONGC Long counter
25 MAGSP Magnetic spectrometer
26 MCPLT Microchannel plate
27 MOXR Moxon-Rae detector
28 MTANK Moderating tank detector
29 MWDC Multi-wire drift chamber
30 MWPC Multi-wire proportional counter
31 MWSC Multi-wire spark counter
32 NAICR Sodium-Iodide crystal
33 PGAC Parallel-grid avalanche detector
34 PHVC Photovoltaic Cell
35 PLATE Nuclear plates
36 PPAC Parallel plate avalanche counter
37 PROPC Proportional counter
38 PS Position sensitive detector
39 PSSCN Position sensitive scintillator
40 PSSSD Position sensitive solid state detector
41 SCIN Scintillation detector
42 SI Silicon detector
43 SIBAR Silicon surface barrier detector
44 SILI Silicon-Lithium detector
45 SISD Silicon strip detector
46 SOLST Solid-state detector
47 SPEC Large spectrometer system
48 STANK Scintillator tank
49 SWPC Single-wire proportional counter
50 TELES Counter telescope
51 TFBC Thin-film Breakdown Counter
52 THRES Threshold detector
53 TPC Time projection chamber
54 TRD Track detector
55 XHPGE Extended range Germanium gamma detector

ion-source

1 A-BE Alpha-Beryllium
2 AM-BE Americium-Beryllium neutron source
3 ARAD Annihilation radiation
4 ATOMI Atomic beam source
5 B11-H 1H(11B,n)
6 BRST Bremsstrahlung
7 CF252 Spont.fission of Californium-252
8 CM-BE Curium-Beryllium neutron source
9 CM244 Spont.fission of Curium-244
10 CM246 Spont.fission of Curium-246
11 CM248 Spont.fission of Curium-248
12 COMPT Compton scattering
13 D-BE 9Be(d,n)
14 D-C12 12C(d,n)
15 D-C14 14C(d,n)
16 D-D 2H(d,n)
17 D-LI Li(d,n)
18 D-LI7 7Li(d,n)
19 D-N14 14N(d,n)
20 D-N15 15N(d,n)
21 D-T 3H(d,n)
22 EVAP Evaporation neutrons
23 EXPLO Nuclear explosive device
24 FRAGM Fragmentation
25 HARD Hardened
26 KINDT Kinematically determined
27 LAMB Lamb-shift source
28 LASER Laser scattering
29 LCS Laser Compton Scattered Photons
30 MPH Monoenergetic photons
31 P-BE 9Be(p,n)
32 P-D 2H(p,n)
33 P-LI7 7Li(p,n)
34 P-N15 15N(p,n)
35 P-T 3H(p,n)
36 PHOTO Photo-neutron
37 PO-BE Polonium-Beryllium neutron source
38 POLIS Polarized ion source
39 POLNS Polarized neutron source
40 POLPS Polarized photon source
41 POLTR Polarized target
42 PU-BE Plutonium-Beryllium neutron source
43 PU240 Spont.fission of Plutonium-240
44 PU242 Spont.fission of Plutonium-242
45 QMPH Quasi-monoenergetic photons
46 RA-BE Radium-Beryllium neutron source
47 REAC Reactor
48 RN-BE Radon-Beryllium neutron source
49 SPALL Spallation
50 TAGD Electron tagged
51 TH-BE Thorium-Beryllium neutron source
52 THCOL Thermal column
53 THRDT Determined by threshold technique
54 VPH Virtual photons

methods

1 ABSFY Absolute fission yield measurement
2 ACTIV Activation
3 AMS Accelerator mass spectrometry
4 ASEP Separation by mass-separator
5 ASPEC Alpha spectrometry
6 ASSOP Associated particle
7 BCINT Beam current integrated
8 BGCT Beta-gamma coincidence technique
9 BSPEC Beta ray spectrometry
10 BURN Burn-up
11 CADMB Cadmium bath
12 CHARG Measurements in gas discharge
13 CHRFL Christiansen filter
14 CHSEP Chemical separation of products
15 COINC Coincidence
16 DIFFR Diffraction
17 DSCAT Double scattering
18 EDE Particle identification by \`E/Delta E\` measurement
19 EDEG Energy degradation by foils
20 EXTB Irradiation with external beam
21 FISCT Absolute fission counting
22 FLUX Neutron flux monitoring
23 FNB Filtered neutron beam
24 FPGAM Direct gamma-ray spectrometry
25 GSPEC Gamma ray spectrometry
26 HADT Heavy atom difference technique
27 HATOM Hot atom method
28 HE-AC Helium accumulation method
29 HEJET Collection by He jet
30 INTB Irradiation with internal beam
31 JET Collection by gas jet
32 LRASY Left-right asymmetry
33 MAGFR Magnetic field rotation
34 MANGB Manganese bath
35 MASSP Mass spectrometry of a product
36 MOMIX Mixed monitor
37 MOSEP Separate monitor foil
38 OLMS On-line mass separation
39 PHD Pulse-height discrimination
40 PHWT Pulse-height weighting technique
41 PLSED Pulse die-away
42 PSD Pulse-shape discrimination
43 RCHEM Radiochemical separation
44 REAC Reactivity measurement
45 REC Collection of recoils
46 REFL Total reflection from mirrors
47 RELFY Relative fission yield measurement
48 RINGR Ring ratio method
49 RVAL R-value measurement
50 SFLIP Spin flip
51 SHELT Shell transmission
52 SITA Single target irradiation
53 SLODT Slowing-down time
54 STATD Statistically determined
55 STTA Stacked target irradiation
56 THERM Gas thermochromatographic separation
57 TOF Time-of-flight
58 TRN Transmission method
59 TTM Thick-target method
60 XSPEC X-ray spectrometry

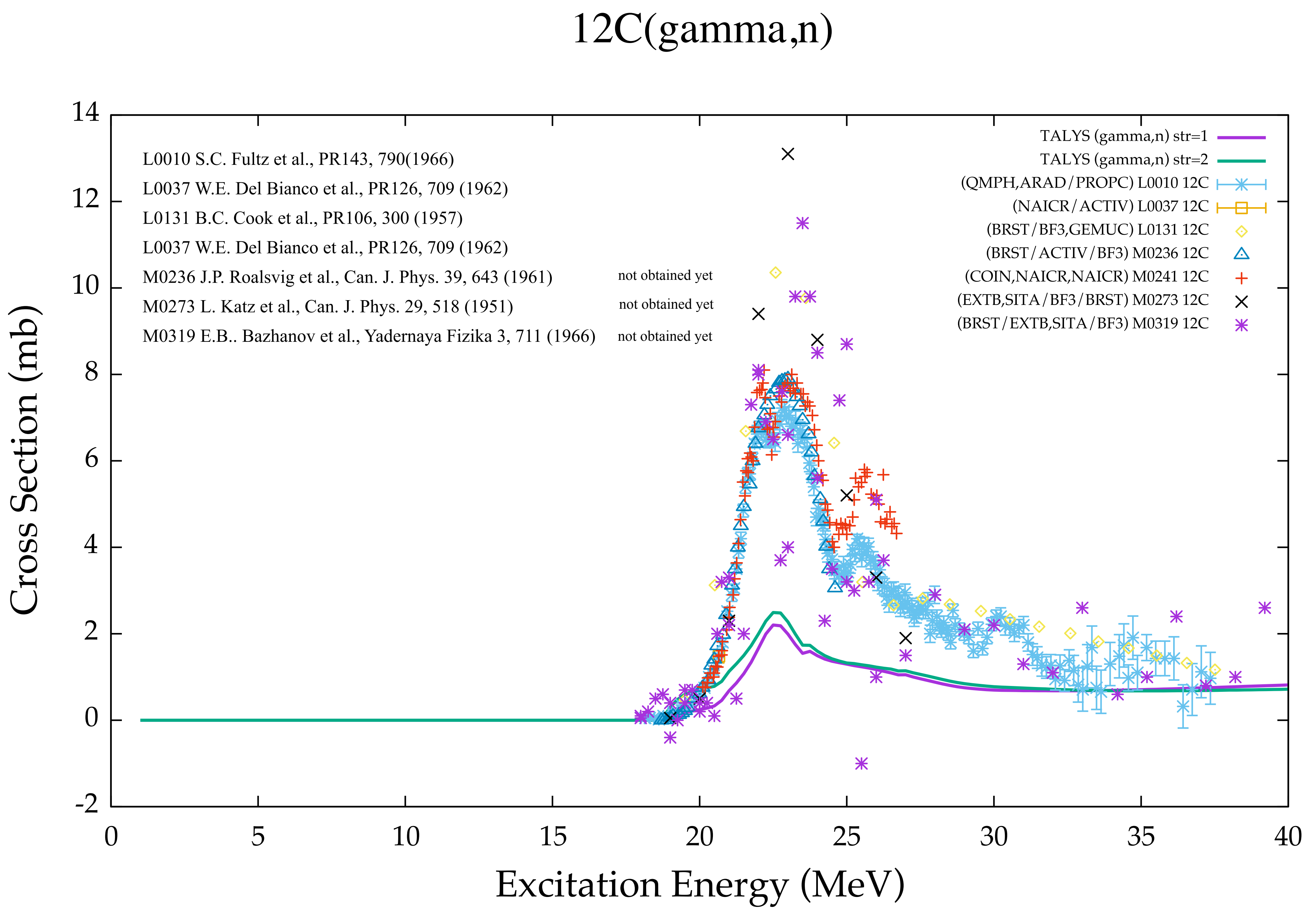
12C(gamma,n)
Cross Section (mb)
Excitation Energy (MeV)
14
12
10
8
6
4
2
0
-2
0
5
10
15
20
25
30
35
40
L0010 S.C. Fultz et al., PR143, 790(1966)
L0037 W.E. Del Bianco et al., PR126, 709 (1962)
L0131 B.C. Cook et al., PR106, 300 (1957)
L0037 W.E. Del Bianco et al., PR126, 709 (1962)
M0236 J.P. Roalsvig et al., Can. J. Phys. 39, 643 (1961) not obtained yet
M0273 L. Katz et al., Can. J. Phys. 29, 518 (1951) not obtained yet
M0319 E.B.. Bazhanov et al., Yadernaya Fizika 3, 711 (1966) not obtained yet
TALYS (gamma,n) str=1
TALYS (gamma,n) str=2
(QMPH,ARAD/PROPC) L0010 12C
(NAICR/ACTIV) L0037 12C
(BRST/BF3,GEMUC) L0131 12C
(BRST/ACTIV/BF3) M0236 12C
(COIN,NAICR,NAICR) M0241 12C
(EXTB,SITA/BF3/BRST) M0273 12C
(BRST/EXTB,SITA/BF3) M0319 12C

(γ,xn)

Gamma-ray source + neutron counting

Gamma-ray source + n-TOF

Gamma-ray source + activation

n-counting

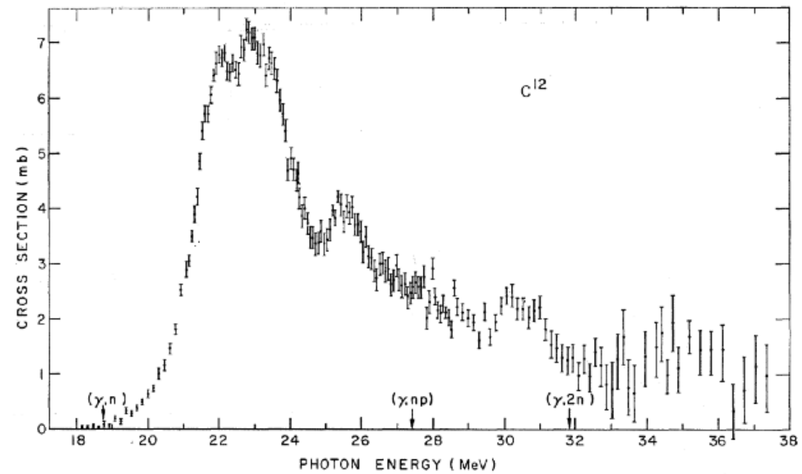

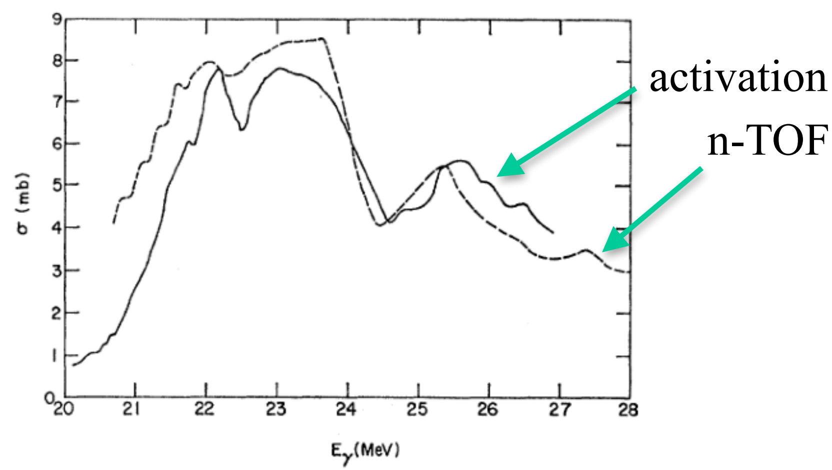

FIG. 4. Comparison of time-of-flight neutron-energy curve (dashed line) of Firk and Bowey with $^{12}C(\gamma,n)^{11}C$ activation curve of present experiment (solid line).

Lawrence Radiation Laboratory, Univ. California, Livermore

positron annihilation in flight

S.C. Fultz et a., PR127, 1273(1962).

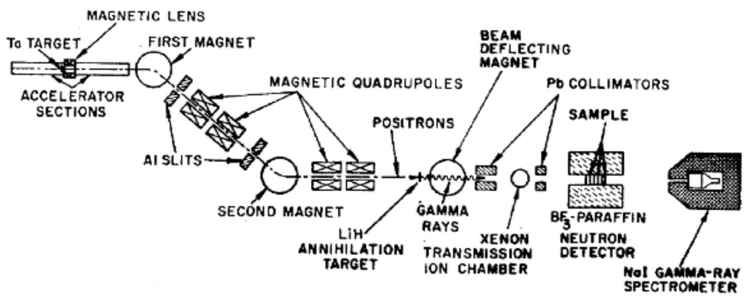

FIG. 1. Experimental apparatus for photoneutron cross-section measurements. The drawing is not to scale. Neutron shields and some gamma-ray shielding have been omitted.

$\Delta E_\gamma / E_\gamma \sim 3\,\%$ at 15.11 MeV

mostly by e$^+$ momentum spread

$$E_\gamma^{\text{peak}} \sim E_{e^+} + 0.76\,\text{MeV} \qquad E_\gamma^{\text{peak}} \simeq E_{e^+} + \frac{3}{2} m_e c^2$$

NaI gamma-ray spectrometer: 6” long, 5”diameter

electron beam at 10 MeV (pulsed)

positron production target: 0.1” thick W or Ta target
— Bremsstrahlung and pair production

positron analysis: 3% momentum resolution

annihilation target of low-mass: Be or LiH
~0.060” thick

sweating magnet

collimator: 6” thick lead, 1.5” diameter aperture

monitor: Xe transmission ion chamber

second collimator

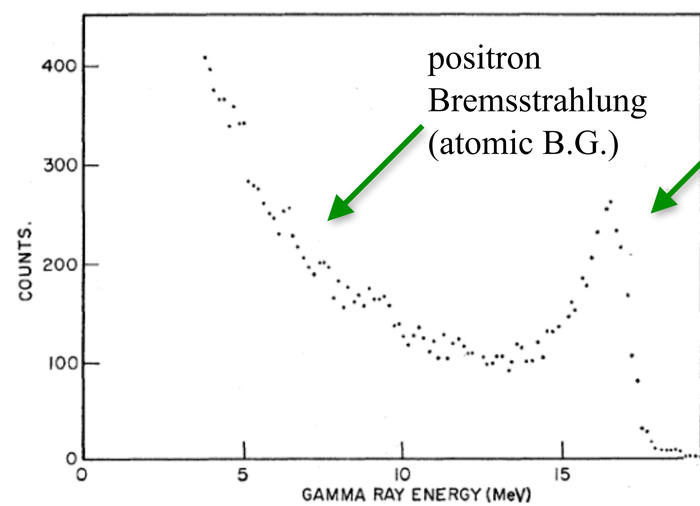

positron annihilation in flight

FIG. 2. Pulse-height spectrum of gamma rays from 15.6-MeV positrons incident on a 0.060-in. thick LiH target.

Lawrence Radiation Laboratory, Univ. California, Livermore

positron annihilation in flight S.C. Fultz et a., PR127, 1273(1962).

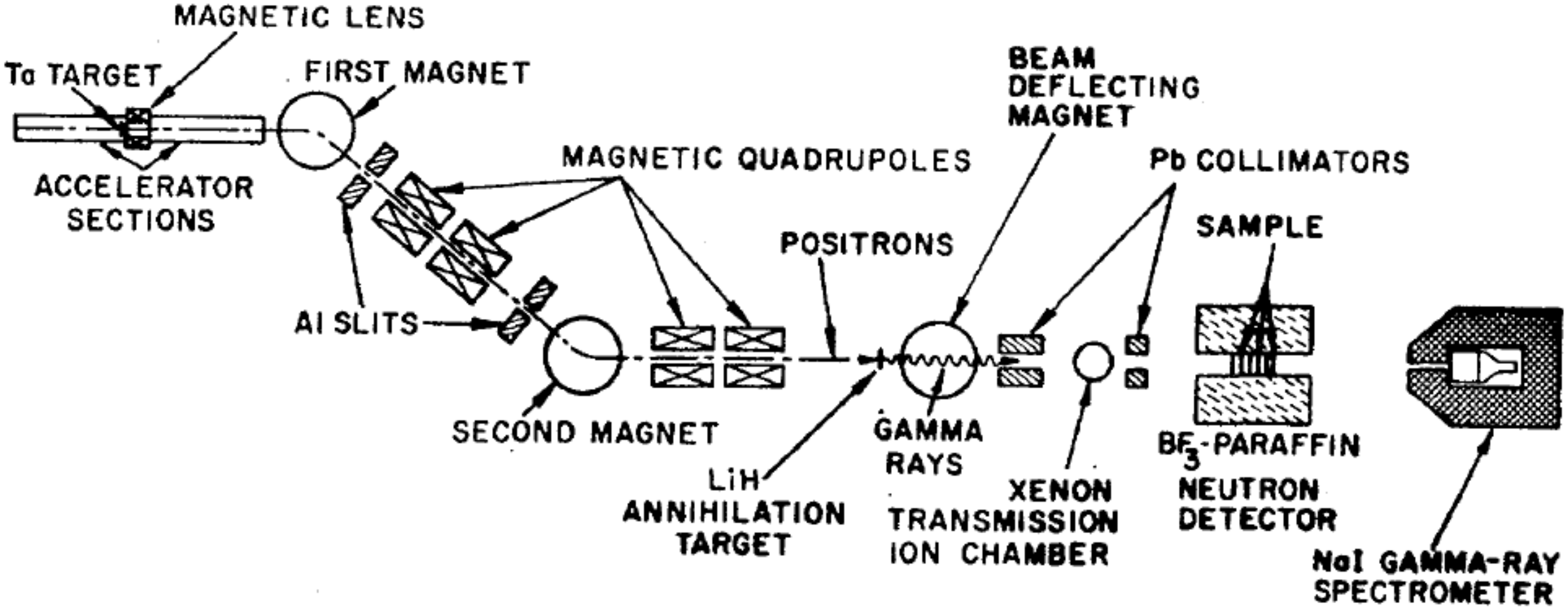

Sacray

positron annihilation in flight

B.L. Berman and S.C. Fultz, Rev. Mod. Phys. 47, 713 (1975)

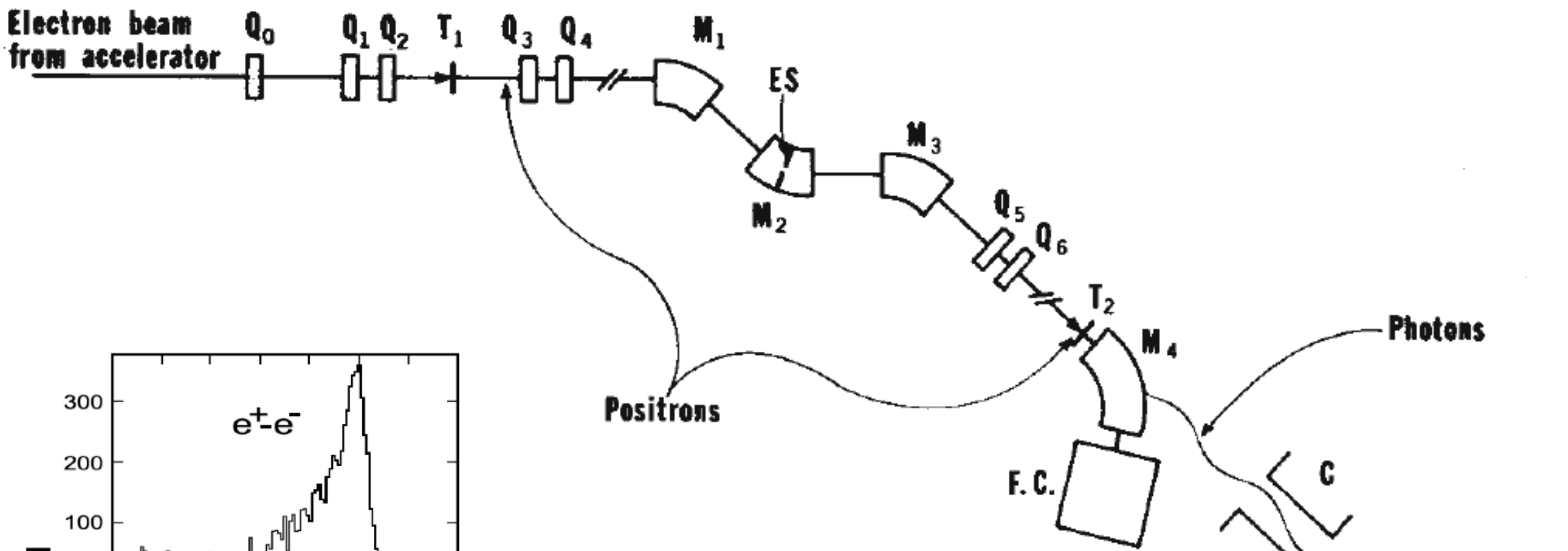

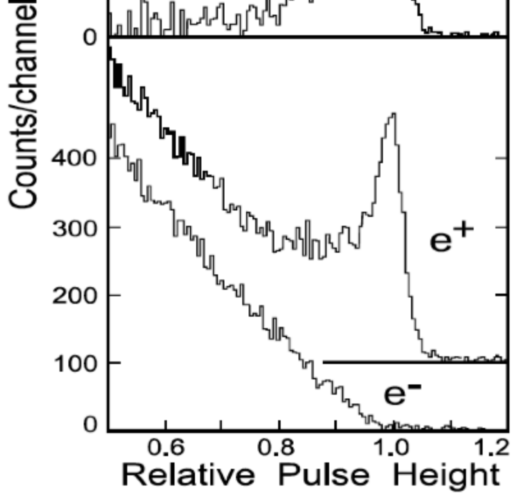

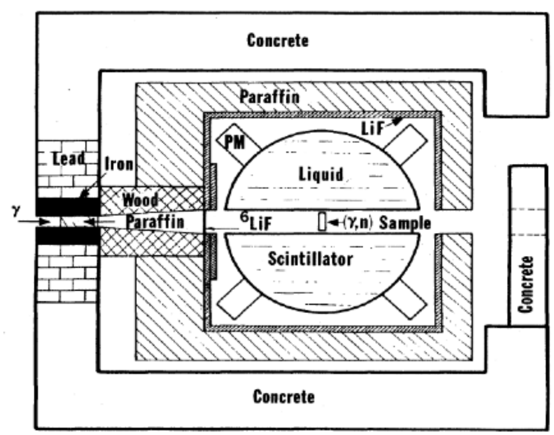

FIG. 7. Cross-section view of the Saclay 4π gadolinium-loaded liquid-scintillator neutron detector and its associated shielding (from Beil *et al.*, 1969).

Lawrence Radiation Laboratory, Univ. California, Livermore

positron annihilation in flight

S.C. Fultz et a., PR127, 1273(1962).

monitor: Xe transmission ion chamber

Xe at 1atm, 1 L

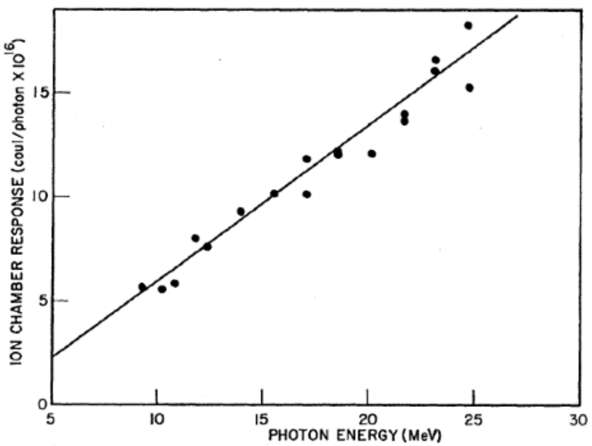

FIG. 3. Typical calibration curve for the 1-liter xenon-filled transmission ion chamber. The charge collected per photon is in units of 10^{-16} C.

no dep. on photon energy?

Target: a stack of 0.25” thick, 2” diameter disks

18 inch^3 4π paraffine modulated neutron detector

24 high-pressure BF_3 counters, two ring structure

essentially the same sensitivity to 0.025, 1.2 and 2.0 MeV neutrons
efficiency ε~0.17

but is not very flat

position beam measurements

flip the magnetic field after pair production

electron beam measurements

subtraction of electron beam data from positron

subtraction of continuous Bremsstrahlung part of the gamma

Number of neutron events were recorded for each of single, double, and triple coincidences.

Lawrence Radiation Laboratory, Univ. California, Livermore

positron annihilation in flight S.C. Fultz et a., PR127, 1273(1962).

4π paraffine modulated neutron detector (BF_3)

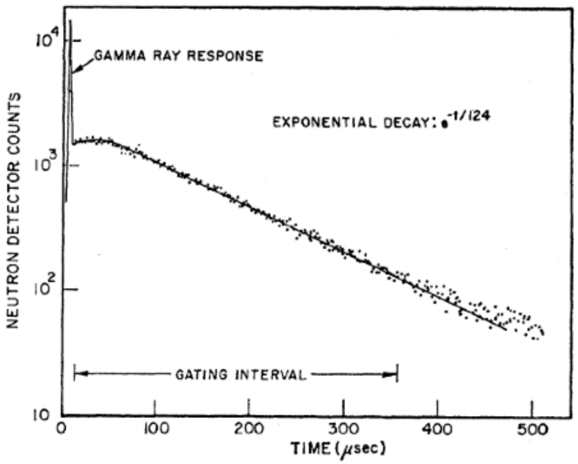

FIG. 5. The characteristic time response curve for the 4π paraffin-moderated neutron detector. The decay period for neutrons was 124 μsec. The sharp peak at the beginning of the curve arises from the response of the BF_3 tubes to the gamma rays.

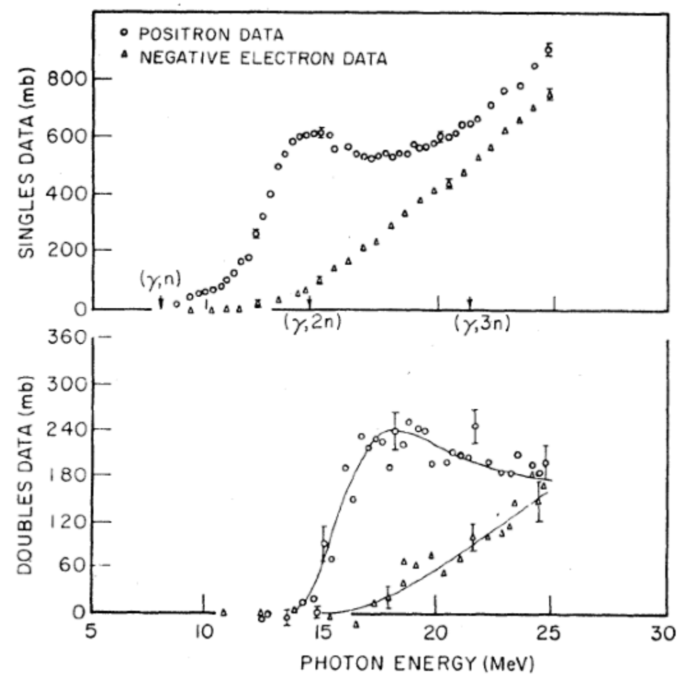

FIG. 6. Partially reduced neutron yield curves for Au. The top set was obtained from counting single neutrons per beam pulse, the lower set from counting two neutrons per beam pulse. For each set of curves, the top curve was obtained by use of positrons while the lower curve was obtained by use of negative electrons.

$$\sigma(\gamma,in)=(N_i/A)(\Omega_\gamma/\Omega_s)\mu/(1-e^{-\mu t})\epsilon_n{}^iN_a,$$

The cross sections were calculated by use of the expression

$$\sigma(\gamma,in)=(N_i/A)(\Omega_\gamma/\Omega_s)\mu/(1-e^{-\mu t})\epsilon_n{}^iN_a,$$

where i denotes the multiplicity, N_i is the number of neutron counts of multiplicity i, A denotes the number of annihilation photons detected, μ is the absorption coefficient in the sample for the nearly monoenergetic photons, t is the thickness of the sample, $\epsilon_n{}^i$ is the efficiency of the neutron counter raised to the power of the multiplicity, N_a is the number of atoms of sample material per cm³, and Ω_γ/Ω_s is the ratio of solid angles subtended at the gamma spectrometer and at the sample, from the annihilation target.

Photo-activation method at Pennsylvania

W.A. Lochstet and W.E. Stephens, PR141, 1002 (1966).

Tandem accelerator

Proton beam above 3.8 MeV, 3-5 μA

T(p,γ)^{4}He reaction for gamma-ray

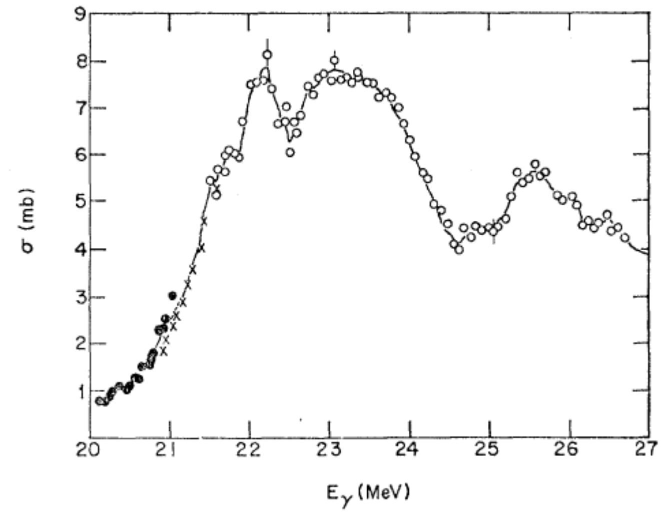

FIG. 3. $^{12}C(\gamma,n)^{11}C$ activation cross-section curve as a function of photon energy.

Activation

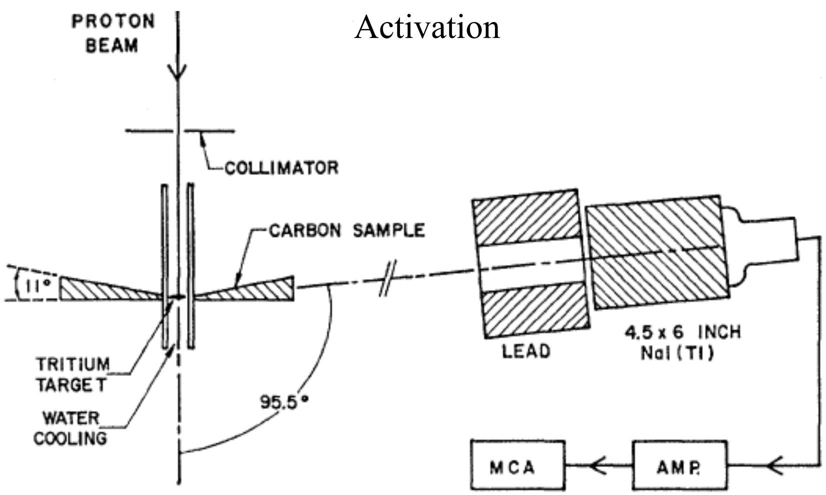

FIG. 1. Schematic experimental arrangement.

Radioactivity measurement from ^{11}C by two NaI in coincidence of two 511 keV gammas

2" thick 5" diameter NaI

n-counting and activation measurement at Enrico Fermi institute

B.C. Cook, PR106, 300 (1957)

Betatron for electron beam

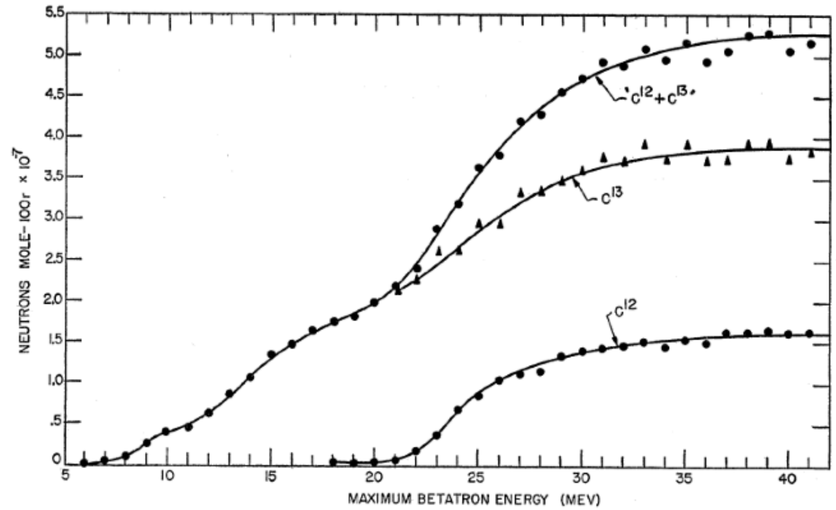

n-counting for $^{12}C(\gamma,n)$

12 enriched $B^{10}F3$ counters (1"diameter - 10" length)

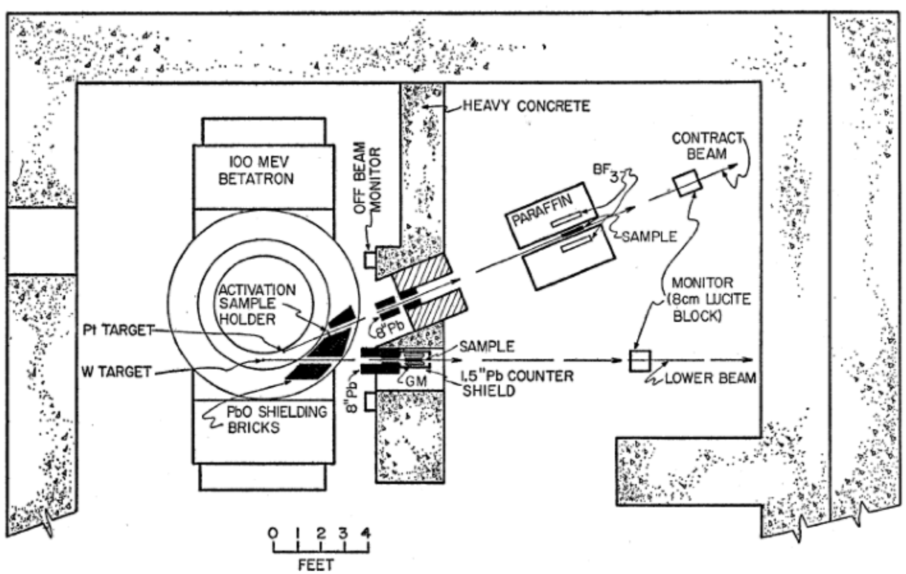

^{11}B radioactivity was measured for $12C(\gamma,p)$ with six GM counter.

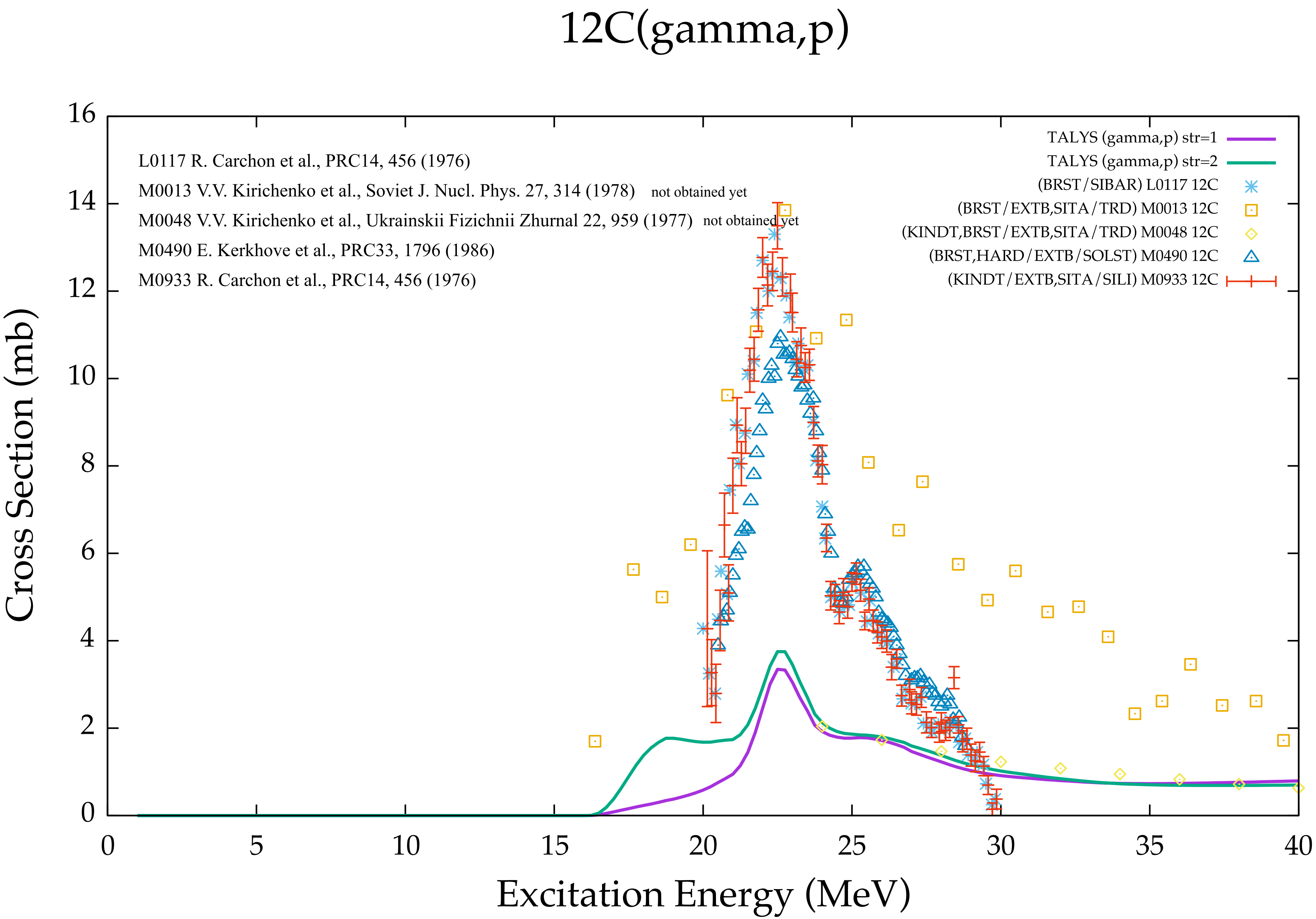

12C(gamma,p)
Cross Section (mb)
Excitation Energy (MeV)
0
2
4
6
8
10
12
14
16
0
5
10
15
20
25
30
35
40
L0117 R. Carchon et al., PRC14, 456 (1976)
M0013 V.V. Kirichenko et al., Soviet J. Nucl. Phys. 27, 314 (1978) not obtained yet
M0048 V.V. Kirichenko et al., Ukrainskii Fizichnii Zhurnal 22, 959 (1977) not obtained yet
M0490 E. Kerkhove et al., PRC33, 1796 (1986)
M0933 R. Carchon et al., PRC14, 456 (1976)
TALYS (gamma,p) str=1
TALYS (gamma,p) str=2
(BRST/SIBAR) L0117 12C
(BRST/EXTB,SITA/TRD) M0013 12C
(KINDT,BRST/EXTB,SITA/TRD) M0048 12C
(BRST,HARD/EXTB/SOLST) M0490 12C
(KINDT/EXTB,SITA/SILI) M0933 12C

(γ,p) measurement at Ghent

L0117 R. Carchon et al., PRC14, 456 (1976)

M0490 E. Kerkhove et al., PRC33, 1796 (1986)

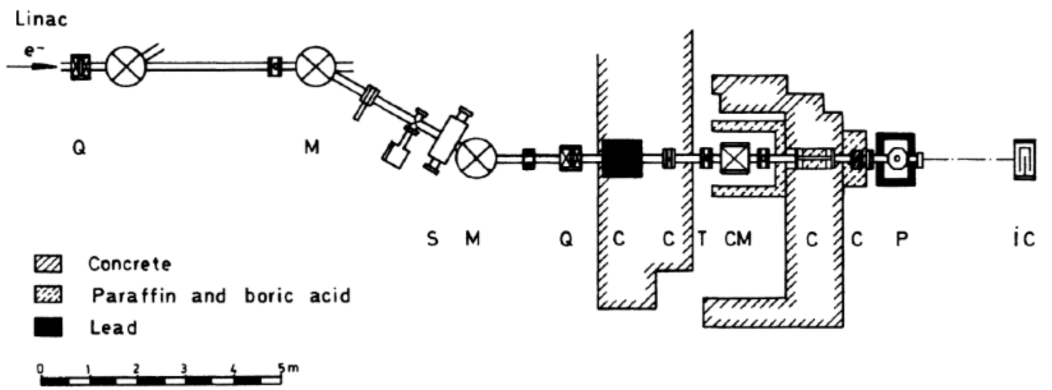

FIG. 1. General layout of the beam transport system and of the experimental arrangement. Q: quadrupole doublet; C: collimator; P: photoproton chamber; M: deflection magnet; T: Bremsstrahlung target; IC: ionization chamber; S: adjustable slit; CM: cleaning magnet.

R. Carchon et al., PRC14, 456 (1976)

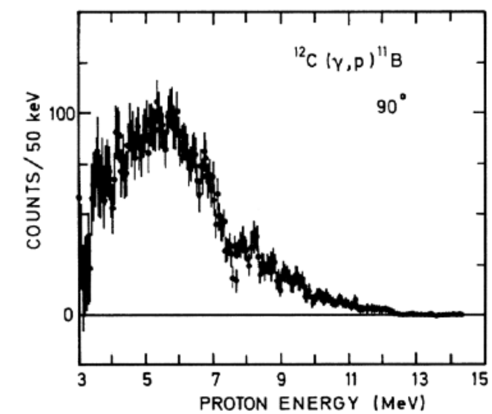

FIG. 3. Photoproton spectrum for the reaction ^{12}C-$(\gamma,p)^{11}$B at 90°, as a function of laboratory proton energy.

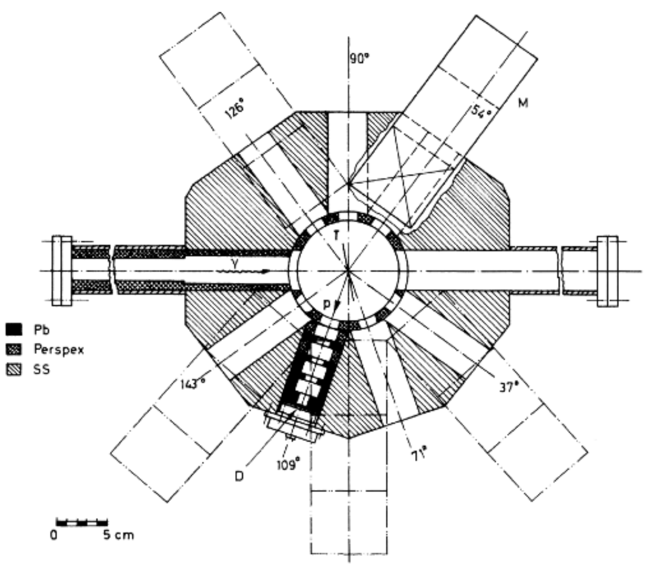

FIG. 2. Schematic drawing of the photoproton detection chamber. T: target; D: detector; M: magnet.

E. Kerkhove et al., PRC33, 1796 (1986)

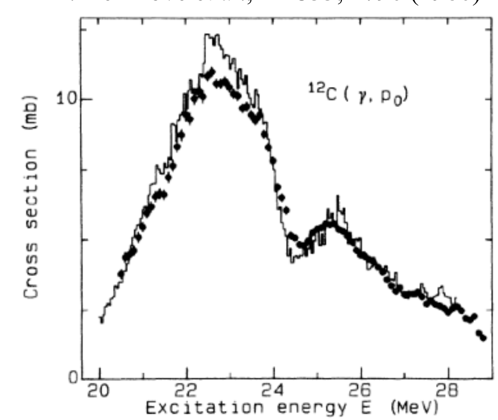

FIG. 1. The absolute total ^{12}C$(\gamma, p_0)^{11}$B cross section obtained in this experiment; the histogram represents the results of the Stanford and Argonne group (Refs. 5–7). The error bars represent the statistical uncertainty only.

(γ,p) and (γ,p_0) measurement at Ghent

E. Kerkhove et al., PRC29, 2061 (1984)

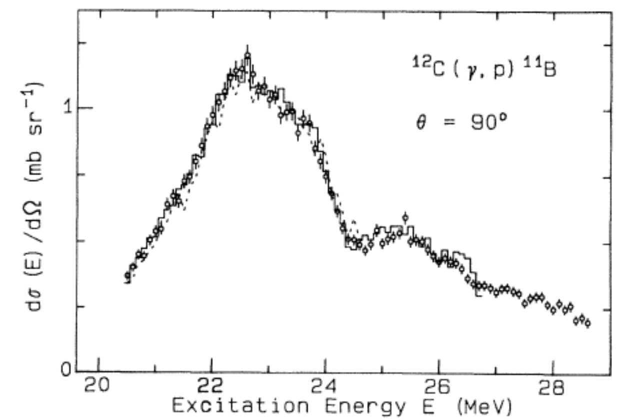

FIG. 6. Comparison of the pseudo-ground-state differential cross sections taken at end point energies of 25 MeV (dashed line), 27 MeV (histogram), and 29 MeV (data points).

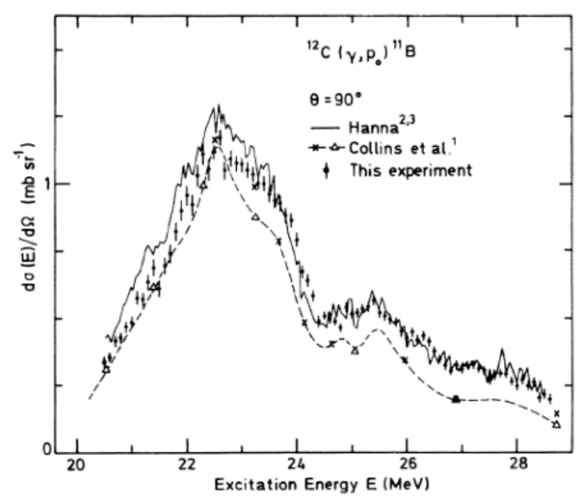

FIG. 7. The absolute 90° differential $^{12}C(\gamma,p_0)^{11}B$ cross section obtained in this experiment, as compared with the results of Collins *et al.* (Ref. 1) (dashed line) and of the Stanford and Argonne group (Refs. 2—4) (full line).

$^{11}B(p, \gamma_0)$ measurement at TUNL and BNL

M.T. Collins et al., PRC26, 332 (1982)

at TUNL, Duke Univ.

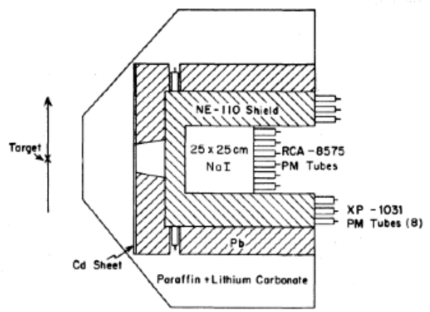

FIG. 1. Schematic of the TUNL γ-ray detection geometry. The shielding in front of the detector consisted of 20.3 cm of paraffin-plus-lithium carbonate (50% mixture by weight), followed by an active plastic scintillator 7.6 cm in thickness.

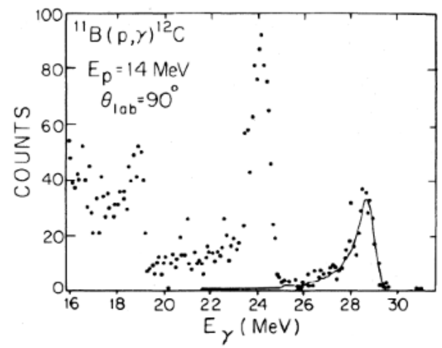

FIG. 2. The $^{11}B(p,\gamma)^{12}C$ spectrum obtained with the TUNL-NaI assembly at $E_p = 14.00$ MeV and $\theta_\gamma^{lab} = 90°$. The solid line represents the intrinsic line shape for the ground state (γ_0) transition (see text).

at BNL

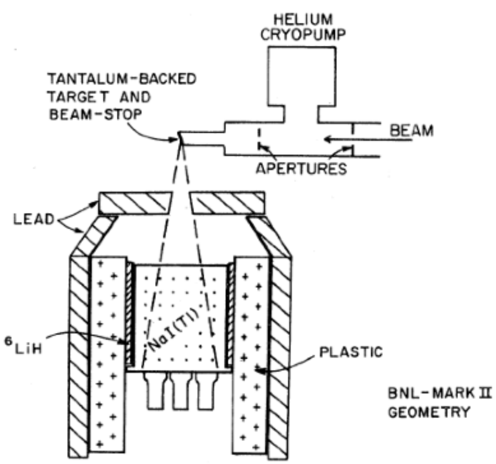

FIG. 3. Schematic of the BNL γ-ray detection geometry.

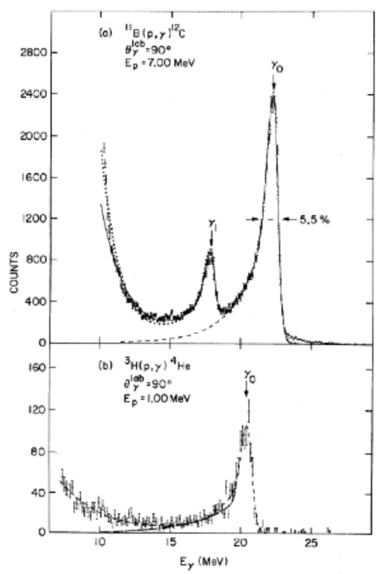

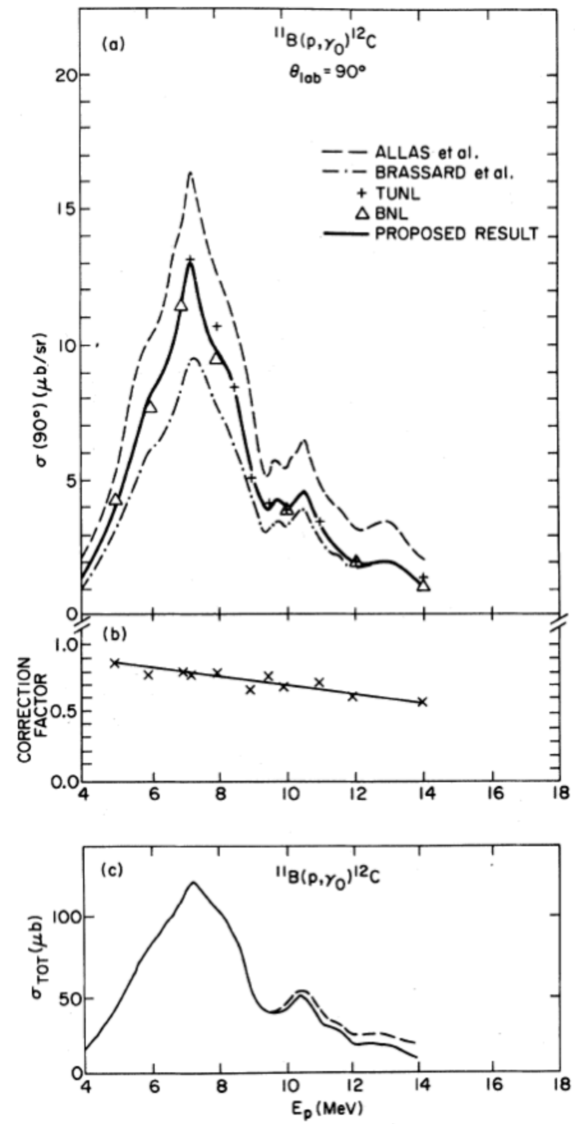

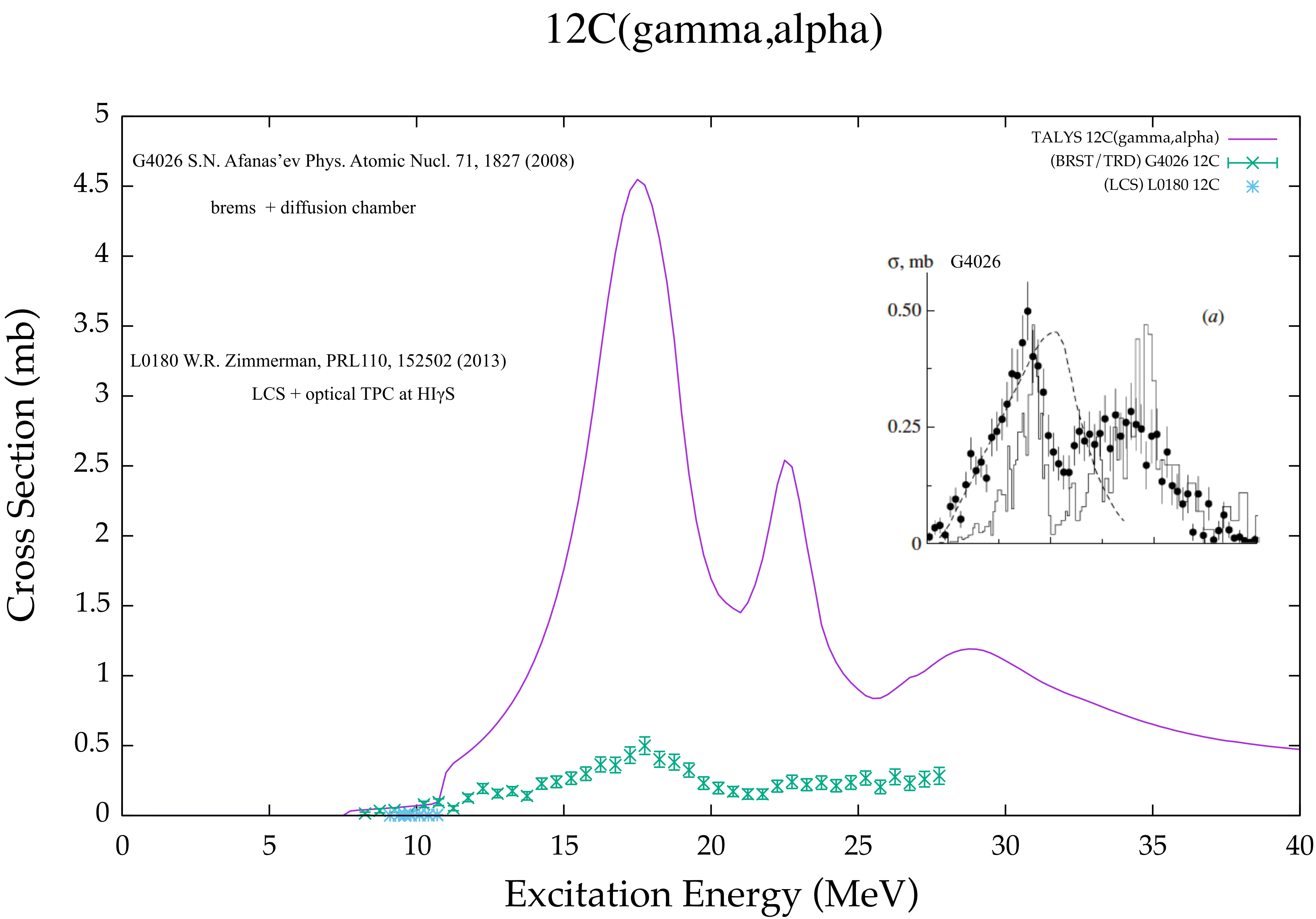
12C(gamma,alpha)
Cross Section (mb)
Excitation Energy (MeV)
G4026 S.N. Afanas'ev Phys. Atomic Nucl. 71, 1827 (2008)
brems + diffusion chamber
L0180 W.R. Zimmerman, PRL110, 152502 (2013)
LCS + optical TPC at HIγS
TALYS 12C(gamma,alpha)
(BRST/TRD) G4026 12C
(LCS) L0180 12C
σ, mb G4026
(a)
0.50
0.25
0
0 5 10 15 20 25 30 35 40
0 0.5 1 1.5 2 2.5 3 3.5 4 4.5 5

Inconsistency between Livermore and Sacray data

T. Kawano et al., Nucl. Data Sheets 163, 109 (2020)

Statements according to New-SUBARU works

(γ,1n) data at Livermore is more reliable than Sacray (Sacray data are too large).

(γ,2n) data at Scary is more reliable than Livermore (Livermore data are too large)

Flat neutron efficiency independent on neutron energy is important.

$$
\begin{aligned}
N_s &= N_1 \varepsilon(E_1) \\
&+ N_2\ {}_2C_1 \varepsilon(E_2)\left\{1-\varepsilon(E_2)\right\} \\
&+ N_3\ {}_3C_1 \varepsilon(E_3)\left\{1-\varepsilon(E_2)\right\}^2 \ .
\end{aligned}
\tag{17}
$$

$$
\begin{aligned}
N_s &= N_1 \varepsilon \\
&+ N_2\ {}_2C_1 \varepsilon(1-\varepsilon) \\
&+ N_3\ {}_3C_1 \varepsilon(1-\varepsilon)^2
\end{aligned}
$$

$$N_d = N_2 \varepsilon^2 + N_3\ {}_3C_2 \varepsilon^2 (1-\varepsilon)$$

$$N_t = N_3 \varepsilon^3$$

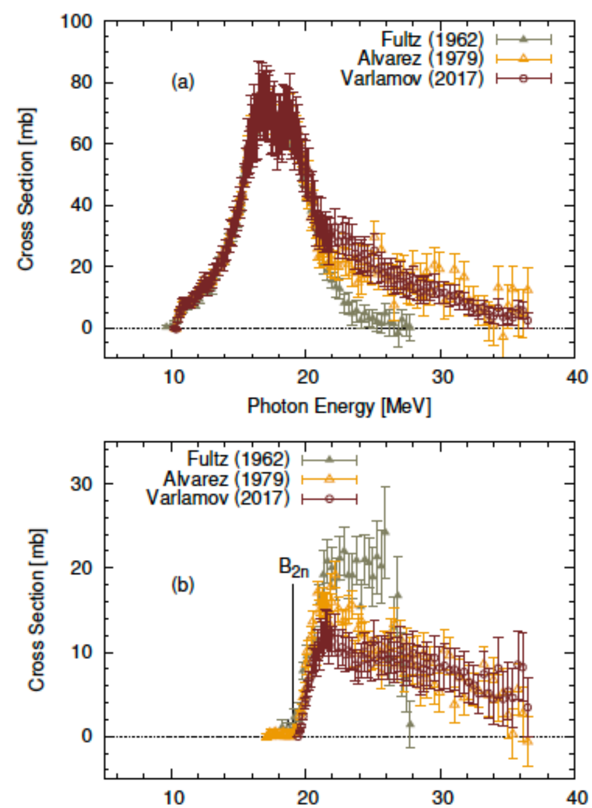

Notes on each method

Bremsstrahlung

The energy distribution is continuous and intensity decreases at higher energy.

Good knowledge of the gamma-spectrum shape is essential and is usually difficult to have.

Precise absolute normalization is also difficult.

Bremsstrahlung-tagging (tagged photon)

Too low in intensity. Only applicable to target of big amount.

Transmission type gamma-absorption measurement

Only applicable to target of big amount.

Correction of atomic absorption (scattering) is significant and makes systematic error large.

Neutron counting

Flat efficiency is essential. Inconsistency between Livermore and Sacray.

Good achievement at New SUBARU.

Activation experiment

Needs to be combined with high-intensity quasi-monoenergetic gamma beam

Notes on each method

($p,\gamma 0$) in inverse reaction

Can be precise and reliable with well calibrated gamma-detectors.

Applicable nuclei is limited (due to abundance and spin-parity)

Only sensitive to the (γ, p_0) channel

(γ, p) and (γ, alpha)

Statistics is requires due to thin target.

With continuous beam, selection of daughter state is difficult. Thus reconstruction of photo-absorption cross section is unachievable.

Thus mono-energetic beam or excitation energy tagging is essential.

Good resolution (<=200 keV) is necessary for avoiding fluctuation by fine structure.

Summary

Quasi mono-energetic gamma-rays or excitation energy tagging is required.

with good resolution

$\Delta E \leq$ 100-200 keV

~30 keV is achievable at RCNP and iThemba LABS

~50 keV mono-energetic beam will be available at ELI-NP

Good absolute c.s. normalization is required.

Good development of monitor detectors at ELI-NP

Systematic measurement at three facilities with reference target (27Al)

Lack of the way of measuring total photo absorption c.s. (for isotopically enriched material) needs to be overcome.

Virtual photon excitation at RCNP and iThemba LABS

Applicability to isotopically enriched (small amount of) target material is required.

Virtual photon excitation is applicable

High-intensity gamma beam at ELI-NP